Multiphoton Fluorescence Lifetime Imaging of Human Hair

ALEXANDER EHLERS, IRIS RIEMANN, MARTIN STARK, AND KARSTEN KÖNIG*
Department of Microsystems/Laser Medicine, Fraunhofer Institute of Biomedical Technology (IBMT), Ensheimer Strasse 48, D-66386 St. Ingbert, Germany

KEY WORDS two-photon microscopy; multiphoton tomography; hair; melanin fluorescence; FLIM; time resolved single-photon counting; eumelanin; pheomelanin

ABSTRACT In vivo and in vitro multiphoton imaging was used to perform high resolution optical sectioning of human hair by nonlinear excitation of endogenous as well as exogenous fluorophores. Multiphoton fluorescence lifetime imaging (FLIM) based on time-resolved single photon counting and near-infrared femtosecond laser pulse excitation was employed to analyze the various fluorescent hair components. Time-resolved multiphoton imaging of intratissue pigments has the potential (i) to identify endogenous keratin and melanin, (ii) to obtain information on intrahair dye accumulation, (iii) to study bleaching effects, and (iv) to monitor the intratissue diffusion of pharmaceutical and cosmetical components along hair shafts. *Microsc. Res. Tech. 70:154–161, 2007.*

INTRODUCTION

Multiphoton microscopy (Hendriks and Lucassen, 2000; König, 2000; Masters et al., 1997, 1998) is an established method for optical examination of biological samples. Because of its inherent sectioning capability 3D images with subcellular resolution can be acquired. With this method the two-photon excited autofluorescence of endogenous fluorophores can be generated. Fluorescent biomolecules are for example reduced nicotinamide adenine dinucleotide (phosphate) [NAD(P)H] coenzymes, metal-free porphyrines, components of lipofuscin, melanin, elastin, and keratin. The extracellular matrix protein collagen generates the second harmonic (SHG) of the incident laser radiation. The combination of the 3D sectioning capability and the luminescence lifetime analysis produces a "4D" image of the sample. Fluorescence lifetime imaging (FLIM) allows the specification of the fluorescent molecules and their microenvironment as well as the separation between SHG radiation and fluorescence with respect to the spatial distribution (Becker, 2005; Bugiel et al., 1989). One powerful application of noninvasive multiphoton imaging is the examination of human skin in vivo (König et al., 2006; König and Riemann, 2003; Richter et al., 2004) in contrast to other optical methods for tissue analysis such as laser-induced breakdown spectroscopy (LIBS) (Corsi et al., 2003) and mass spectrometry (Hallégot et al., 2004), which require tissue removal and sample destruction. Raman spectroscopy typically needs long exposure times and does not provide high in vivo spatial resolution so far (Caspers et al., 2001).

The human hair is the most investigated skin appendage. Electron microscopy and chemical analysis have been performed to characterize structure and chemical composition e.g., for the cosmetics industry (Zahn, 1984).

The structure of hair is described by Zahn (1984) and Van Neste (2003). Hair is a skin appendage emerging from the follicle, a tubular invagination of the skin. The hair shaft itself is a keratinized structure composed of three layers. The outer layer is called cuticle and is a tile-like protective layer of keratinized cells with a thickness of about 5 μm. The bulk of the hair, the cortex, consists of spindle structures with lengths of about 100 μm. These are composed of smaller cell structures, the macrofibrils. The innermost layer is called medulla. In the medulla the cells are larger, less tight connected and partially separated by air spaces. The medulla is present in thick hair only. Typical average diameters of a human hair are between 55 and 85 μm. The cross-section is elliptical. Figure 1 represents a scheme of human intratissue hair. Melanin granules are responsible for the coloration of hair. Of the four different types of melanin, eumelanin, pheomelanin, and neuromelanin, only the former two can be found in human hair. Pheomelanin is predominant in blond and red hair, whereas eumelanin is a major part in black and brown hair. The melanin granules are arranged in ellipsoid-like melanin granules with a size of about 0.8–1.0 μm × 0.3–0.4 μm, the long axis is parallely aligned to the cortex fibers (Ulrich et al., 2004).

Multiphoton fluorescence imaging and FLIM of human hair offer the possibility of in vivo examination of pathological and cosmetical alterations as well as bleaching and diffusion effects. Because of the nondestructive character a monitoring of the same sample over long time is possible. Within this work we report on in vivo and in vitro multiphoton studies on human hairs with and without staining.

MATERIALS AND METHODS

Multiphoton Imaging Systems

The multiphoton tomograph DermaInspect (JenLab, Jena, Germany, Fig. 2) was used for in vivo and in vitro studies (König and Riemann, 2003). The system is based on a compact, femtosecond titanium: sapphire

*Correspondence to: Karsten König, Fraunhofer Institute of Biomedical Technology (IBMT), Ensheimer Strasse 48, D-66386 St. Ingbert, Germany.
E-mail: karsten.koenig@ibmt.fraunhofer.de

Received 23 March 2006; accepted in revised form 1 July 2006

DOI 10.1002/jemt.20395

Published online 6 December 2006 in Wiley InterScience (www.interscience.wiley.com).

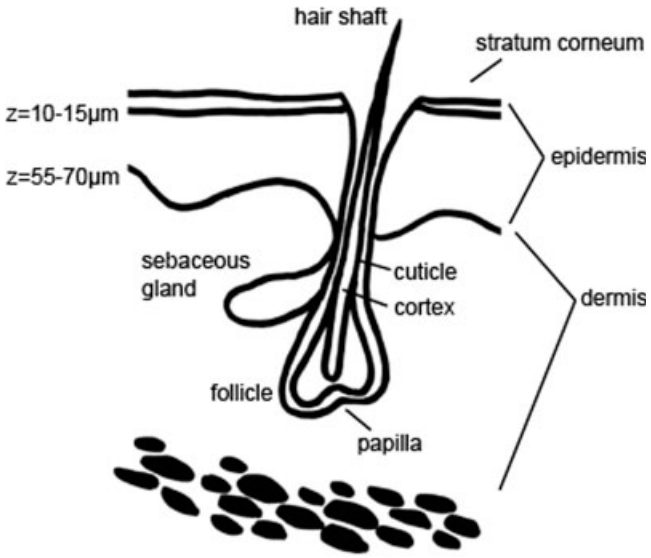

Fig. 1. Scheme of an intratissue hair with typical length parameters of a forearm of a female volunteer.

laser (Chameleon, Coherent) with tunable wavelength between 720 and 930 nm (NIR region), a maximum laser output of about 1 W, 150 fs pulse width, and 90 MHz repetition rate. Various detectors have been employed such as the photomultiplier tubes (PMT) H5773P and PMH100 consisting of a Hamamatsu H5773 photosensor module and a preamplifier with a time spread (FWHM) of 200 ps. To be able to get a better time resolution for fast fluorescence decays, an R3809U-50 multichannel plate (MCP) (Hamamatsu, Japan) with a time spread of 24 ps (FWHM) was used. Focusing of the laser was performed by a 40× focusing optics with NA 1.3 (oil) with a working distance of 200 μm as well as a 20×/NA0.9 (water) optics with a working distance of 2 mm. The piezo-driven stage to move the objective in axial direction had an accuracy of 40 nm and a working distance of 400 μm. Images were obtained with scan times of 1–25 s per frame. The system was further equipped with a 700-nm-shortpass filter to prevent scattered or reflected light from the samples entering the detector.

For in vitro studies of biopsies and individual hair samples, the picosecond multiphoton fluorescence lifetime microscope TauMap (JenLab) was used. It consists of a compact inverted laser microscope with an attached galvo-scanning unit. The same laser source and detectors as described above were employed (Ulrich, 2004).

Fluorescence lifetime imaging (FLIM) was performed by time-resolved single-photon counting (TCSPC) (Becker, 2005; Bugiel et al., 1989). The PMT signal was synchronized with the beam position on the sample and recorded with a TCSPC-module (SPC-830, Becker & Hickl, Germany). Images with 128 × 128 pixels were obtained. Every pixel of such an image contained a complete fluorescence lifetime decay curve. The recorded intensity $I(t)$ measured by the detector is a convolution of the fluorescence decay $F(t)$ with the instrumental response function. The curve fitting as well as the calculation of histograms was performed with the software package included in the TCSPC module. A biexponential fit to the measured fluorescence decay curves was used. The fitting parameters were mapped in a color-coded image. The histograms of the maps show the distribution of the fitting parameters and offer another tool to analyze the sample. In this work we concentrated on the examination of the distribution of the lifetimes τ_1 and τ_2. For comparison of lifetime distributions measured in different samples, every distribution was normalized to the number of pixels of the respective image. The response function $R(T)$ was determined by measuring the SHG signal of collagen from bovine tendons (Sigma, Germany) using a laser wavelength of 840 nm. Since SHG is an instant process, the intensity signal measured by the detector shows the response time of the detection system. The time resolution (FWHM) was determined to be 24 ps for the R3809U-50 MCP and 200 ps for the PMH100.

Sample Preparation

In vivo studies on intradermal hairs and pigmented lesions (nevi) have been performed on human forearms (Caucasian skin type 2). Hair samples for studies were removed from human Caucasian skin type volunteers aged between 20 and 50 years with black, red, blond, and gray hair. The samples were placed on a microscope slide with water, sealed with a coverslip, and imaged immediately after preparation.

For comparative studies, samples of artificial melanin (DOPA-melanin, Sigma) in distilled water (0.1 mg/mL) were prepared.

RESULTS AND DISCUSSION

Multiphoton Imaging

In vivo multiphoton measurements of human skin show strong keratin fluorescence of the hexagonal shaped cells of the stratum corneum, NAD(P)H fluorescence of the living cells within stratum granulosum and spinosum, and within the dermis elastin autofluorescence and SHG of collagen. Basal cells show an intense luminescence because of NADH and melanin. Remarkably, human hairs exhibited a brighter fluorescence compared with the skin cells and the proteins of the extracellular matrix. We were able to detect hair structures based on near-infrared excited luminescence down to an intratissue depth of 400 μm, which corresponds to the working distance of the piezo-driven stage. However, high contrast images could typically be obtained to a depth of 250 μm. Figure 3 shows the bright fluorescence of a single hair embedded in cells of the stratum corneum. To obtain the same fluorescence intensity (photons/pixel) as in the case of the cells, the laser power had to be reduced by a factor of two (Fig. 3b). Figure 4 shows images out of a stack of multiphoton sections obtained in z-steps of 10 μm.

Next, studies of single hair have been performed. The hair structures cortex, cuticle, and medulla could be clearly distinguished based on multiphoton luminescence. As seen in Figure 5, the cuticle exhibited the characteristic tile-like structure. Each tile gives rise to a strong fluorescent signal representing a structure of very closely packed fluorescing cells. According to this image, the thickness of the cuticle could be determined to be 6 ± 2 μm. The inner fibrous structure of the cortex is shown in depths of 15 and 25 μm. The resolution

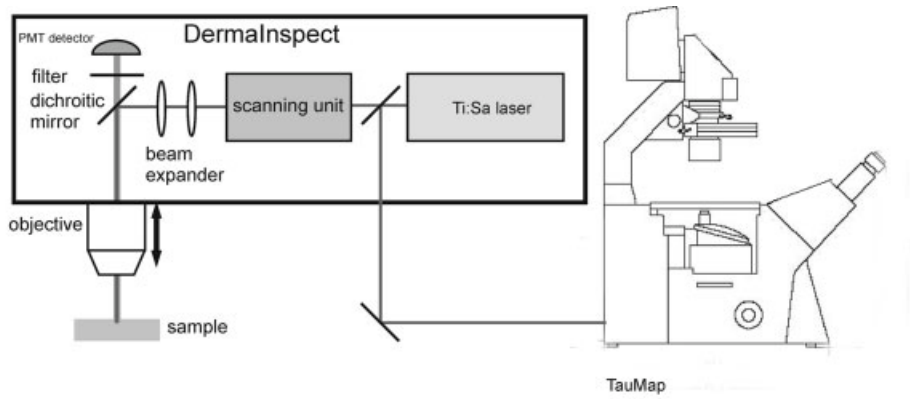

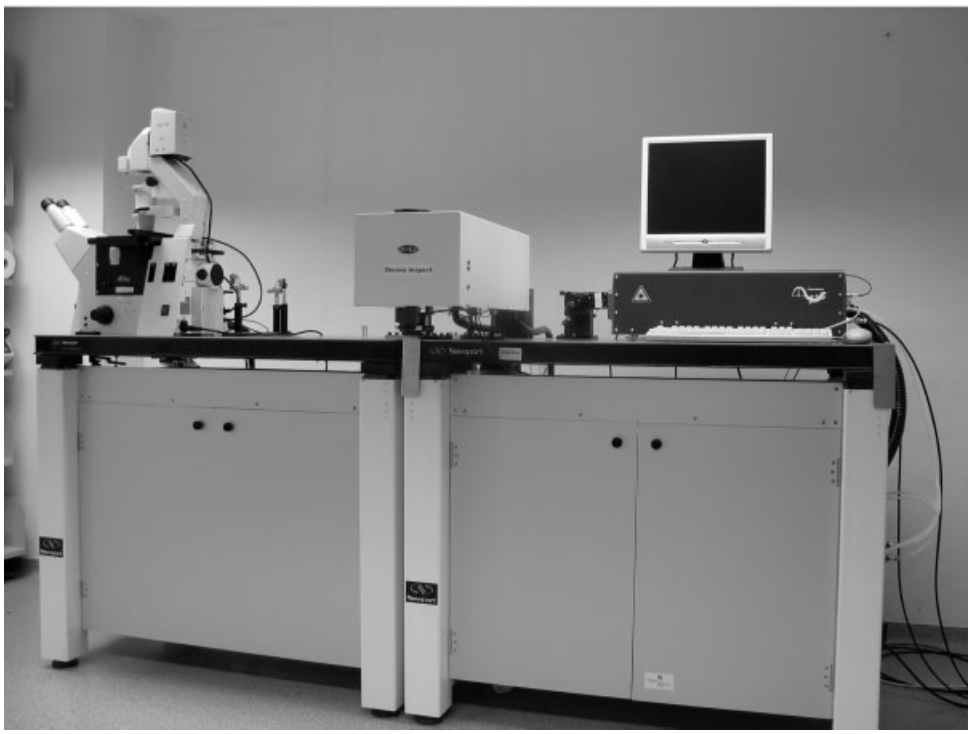

Fig. 2. The multiphoton tomograph DermaInspect and the multiphoton fluorescence lifetime microscope τ-map.

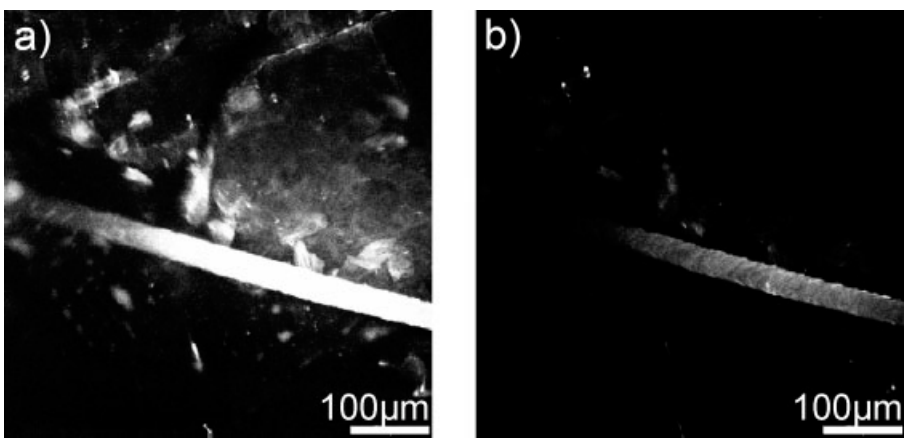

Fig. 3. In vivo multiphoton image of single hair embedded in stratum corneum of a female human volunteer.

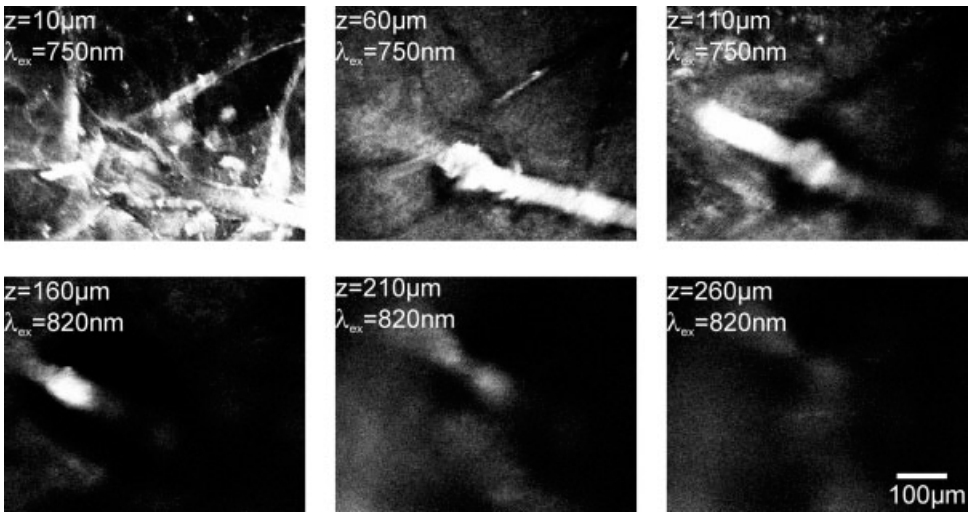

Fig. 4. In vivo images out of a stack of multiphoton sections obtained in z-steps of 10 µm showing a hair follicle in the epidermis and dermis. Upper three images: λ_{ex} = 750 nm, lower images λ_{ex} = 820 nm.

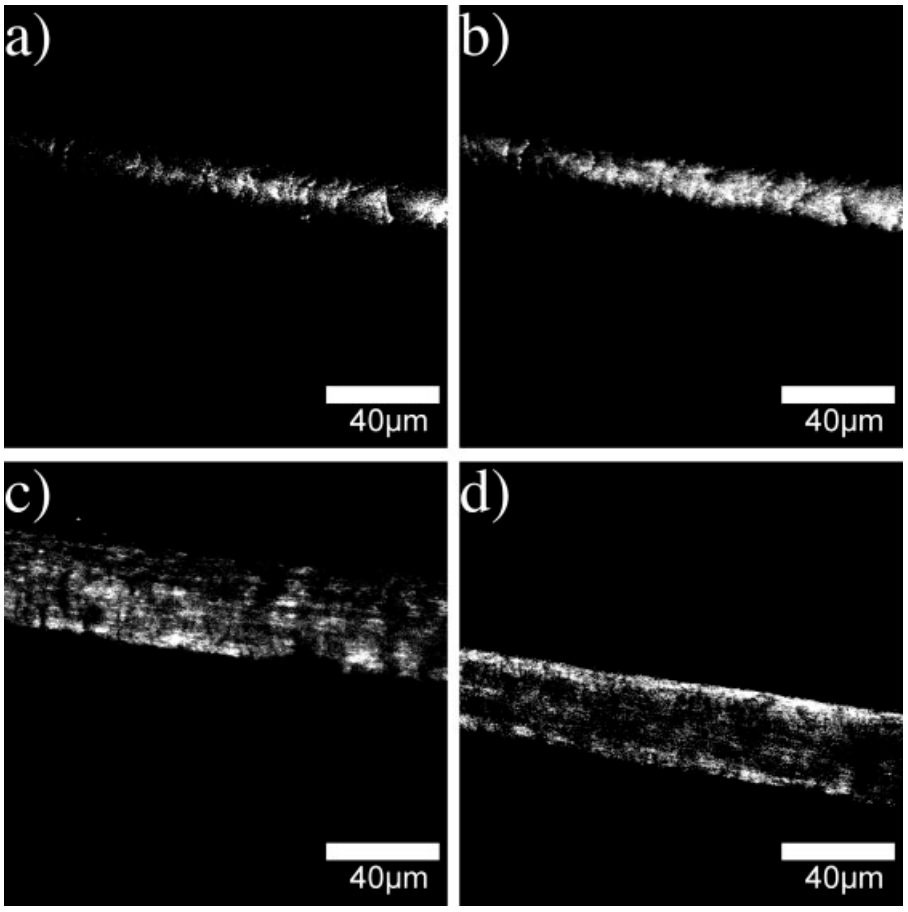

Fig. 5. Multiphoton image of blond human hair. λ_{ex} = 750 nm, imaging depths: (**a**) z = 1 µm, (**b**) z = 5 µm, (**c**) z = 15 µm, (**d**) z = 25 µm.

was insufficient to distinguish further between the small macro fibrils. Some elongated areas of the hair fibers with a size of 3–6 µm gave rise to a relatively strong fluorescent signal. The thickness of cortex fibers was determined to be 1–1.4 µm.

In the cases of blond and red hair, the fluorescence intensity was relatively homogeneously distributed over the whole hair. However, the hair fibers could be clearly identified. In the case of black hair, the multiphoton fluorescence showed a different pattern. The outer parts belonging to the cuticle exhibited a strong fluorescence signal in comparison with the cortex. The signal from the fibrous structure was almost near the detection limit. The origin of the different fluorescence behavior between black and blond/red hair was further investigated by FLIM measurements.

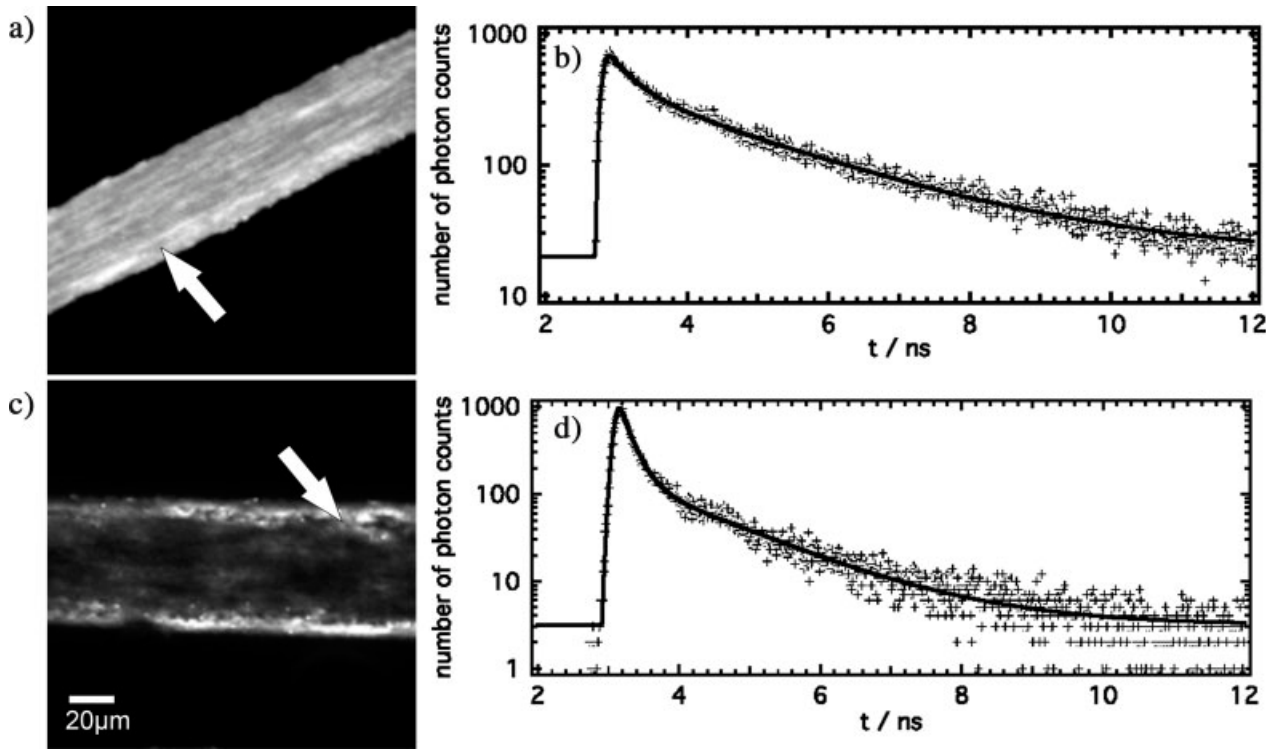

Fig. 6. Fluorescence lifetime imaging of blond and black human hair. (**a**) False-color-image of the long decay time τ_2 of blond hair. The arrow shows the place for which the typical lifetime decay curve is given (**b**). (**c**), (**d**) black hair, same imaging depth.

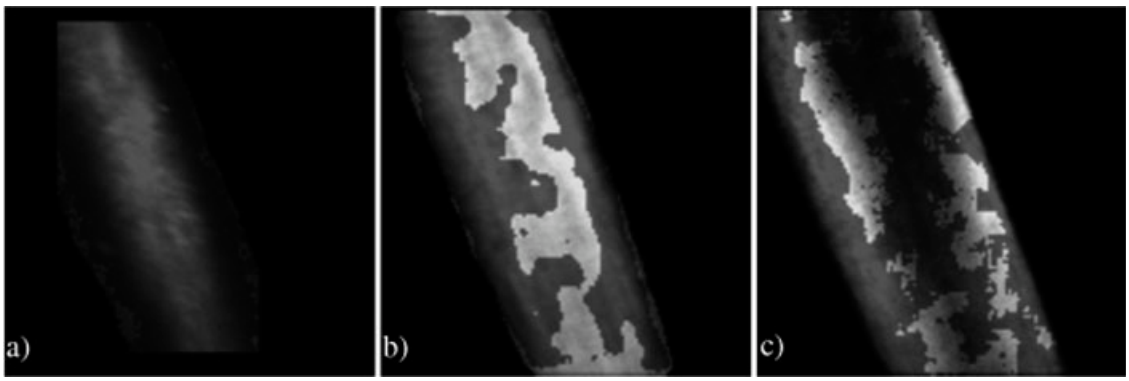

Fig. 7. Fluorescent lifetime images of black human hair. Imaging depths: (**a**) $z = 5$ µm, (**b**) $z = 15$ µm, (**c**) $z = 25$ µm. The bright gray color corresponds to lifetimes $\tau_2 < 1$ ns, dark gray to $\tau_2 > 1$ ns.

Fluorescence Lifetime Imaging

Compared with multiphoton stationary fluorescence microscopy, the map of lifetime data provided the same spatially resolved features. In addition, FLIM imaging offers the possibility to distinguish between different fluorophores. All fluorescent domains in human hair appeared as multicomponent system. We did not find areas of clear monoexponential decay. In contrast, pure keratin samples provided by the company Sigma exhibited monoexponential decay characteristics with a decay time of 1.4 ns.

Figure 6 presents fluorescence lifetime images of blond and black human hair. The images were recorded in a depth of $z = 20$ µm and show the grayscale coded map of the lifetime τ_2, The gray values are scaled from 0.5 ns (black) up to 2.5 ns (white). In the same figure, two respective fluorescent lifetime decay curves from particular pixels depicted by the arrows are shown. A biexponential fitting curve yielded the parameters $\tau_1 = 0.4$ ns, $A_1 = 53\%$ and $\tau_2 = 2.2$ ns, $A_2 = 47\%$ in the case for the blond hair and $\tau_1 = 0.2$ ns, $A_1 = 90\%$, and $\tau_2 = 1.3$ ns, $A_2 = 10\%$ in the case for the black hair.

Different intratissue areas within blond hair showed nearly the same lifetime decay of $\tau_2 = 2.2$ ns with full-width at half maximum (FWHM) of 0.2 ns. The fiber structure was clearly visible. For black hair, the lifetime distribution in the cuticle was found to be different from

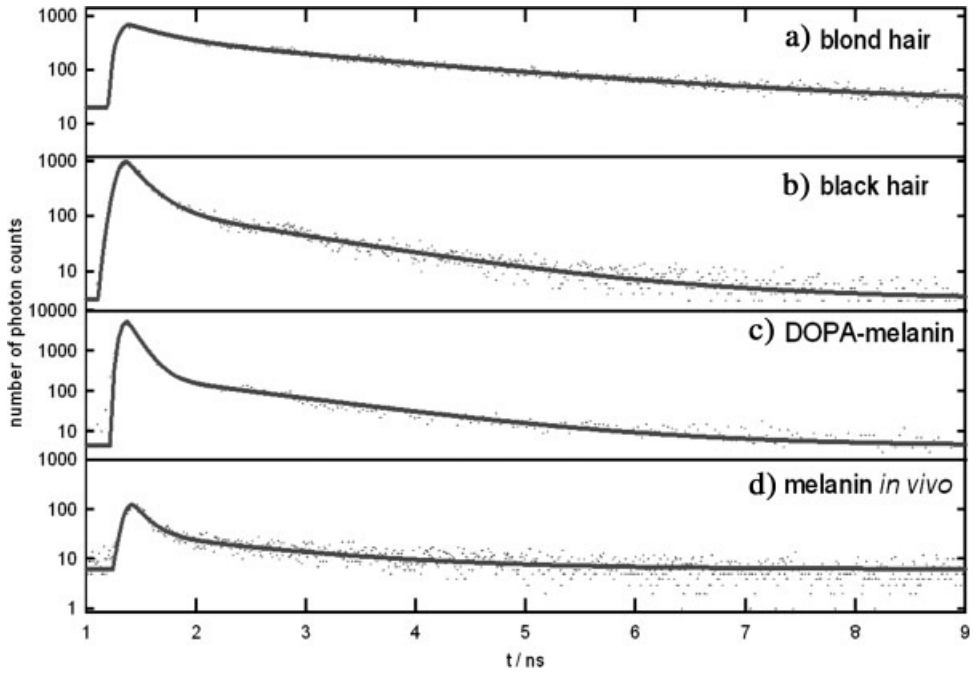

Fig. 8. Typical lifetimes of fluorophores: (**a**) blond hair, (**b**) black hair, (**c**) artificial DOPA melanin, and (**d**) melanin found in human nevi (melanozytes) in vivo.

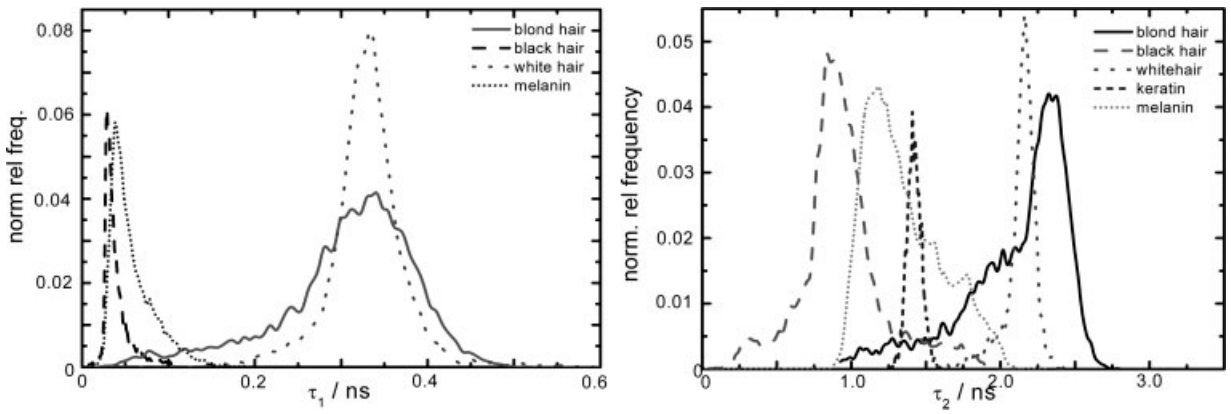

Fig. 9. Normalized histograms for the distribution of the fluorescent components τ_1 and τ_2 of blond and black hairs, keratin, and melanin in vivo.

the cortex. In addition, the fluorescence lifetimes changed with imaging depth (Fig. 7). Fluorophores in cuticle ($z = 5$ μm) had a typical τ_2 lifetime component of more than 1 ns whereas the upper cortex areas ($z = 15$ μm) exhibited τ_2 lifetimes less than 1 ns. In deeper areas of the cortex ($z = 25$ μm) the τ_2 lifetimes increased to values more than 1 ns. This leads to the assumption that eumelanin is responsible for the regions with a short τ_2 lifetime since the melanin granules are mostly found in the inner parts of the cortex, whereas the longer τ_2 values can be attributed to keratin in the cuticle and in the cortex fibers.

In Figure 8 typical lifetime decay curves of blond and black hairs, keratin, artificial melanin (DOPA-melanin), and melanin in vivo are displayed. Black hair and both melanin types show a very dominant ($A_1 > 80\%$) fast component τ_1. In all these cases this component is in the range of the IRF of the system with the PMT PMH100. To be able to determine the fast lifetimes more accurately, we employed the faster detector R3809U-50 MCP with its small time spread of 24 ps (Fig. 9). The fast decay components show a clear distinction between the different hair colorations. Black hair with eumelanin showed a short and narrow τ_1 lifetime distribution with a peak at 0.03 ns (FWHM 0.03 ns). This is similar to the lifetime decay characteristics found for DOPA melanin with a peak at 0.04 ns (FWHM 0.03 ns). For red and blond hair containing pheomelanin, the τ_1 lifetime distribution appeared to be broader with a peak at 0.34 ns (FWHM 0.12 ns) and an elongated shoulder.

The analysis of the lifetime distribution (histograms) as an alternative analytical tool to FLIM images was also performed for the long fluorescence component τ_2. The distribution of the slow components showed also a clear distinction between hair types. Blond hair exhibited a peak at 2.3 ns (FWHM 0.3 ns), whereas black

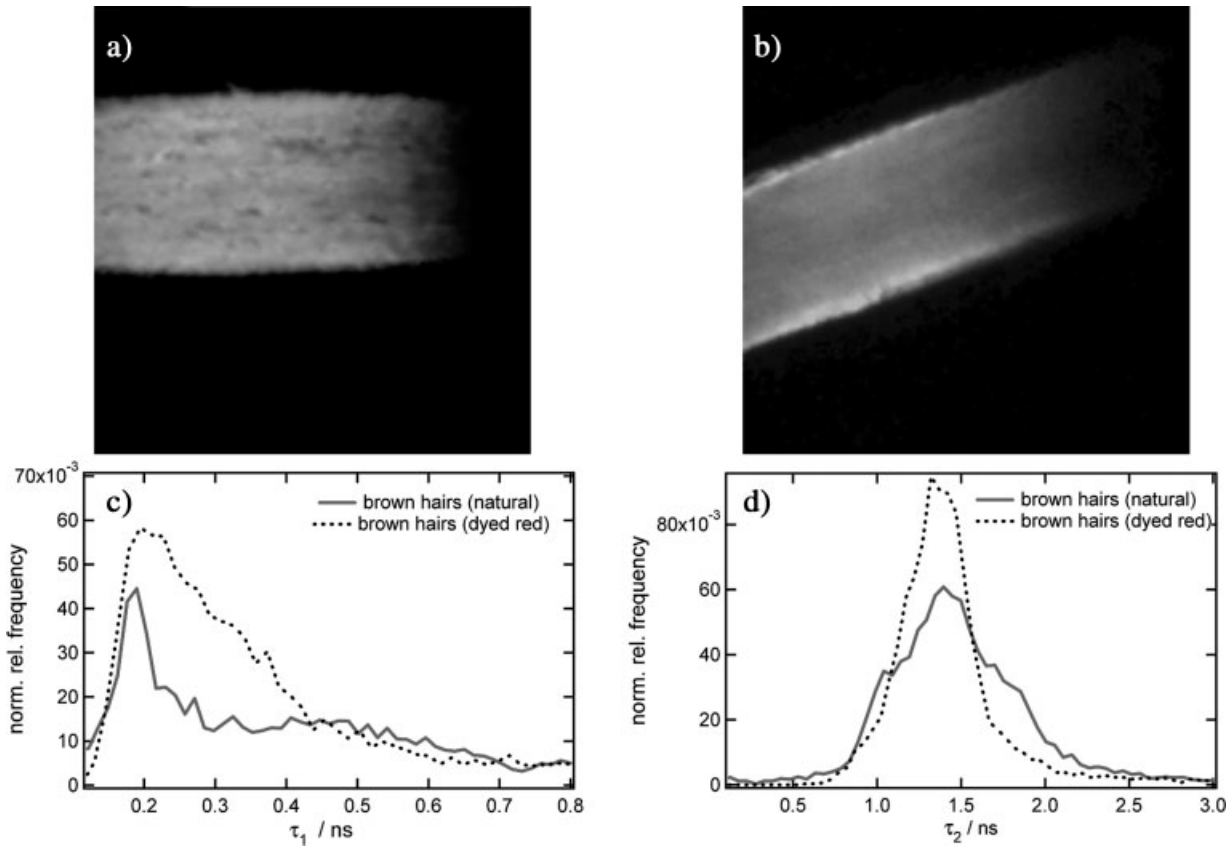

Fig. 10. FLIM images of dyed hair: (**a**) original brown hair, (**b**) hair dyed red, (**c**) τ_1 distribution, and (**d**) τ_2 distribution.

hair had a peak at 0.8 ns (FWHM 1.3 ns). The slow DOPA-melanin lifetime showed a peak at 1.2 ns (FWHM 0.4 ns) and keratin of 1.4 ns (FWHM 0.1 ns). Artificial keratin exhibited a very narrow distribution compared with pheomelanin.

The Figure 9 represents also lifetime distributions of white hair, which is characterized by a lack of melanosomes (Commo et al., 2004). The original hair color was blond. The peaks of the distributions were found to be at $\tau_1 = 0.3$ ns (0.06 ns FWHM) and $\tau_2 = 2.1$ ns (0.1 ns FWHM). A hair with no melanosomes would have a fluorescence lifetime distribution similar to keratin (1.4 ns). It is very likely that the investigated hair contained still small amounts of melanin.

Artificial Hair Coloration

Of further interest is the analysis of the influence of chemical components on hairs. As an example, we examined the difference between the fluorescence behavior of a dyed hair ("Lava red," L'Oreal) compared with nonstained brown hairs of the same volunteer Figure 10 represents an color-coded image based on τ_2 data as well as lifetime distributions. The peaks of the distributions of the dyed hair where found to stay at the same valus at about $\tau_1 = 0.2$ ns and $\tau_1 = 1.3$ ns. However, the FWHM of the distributions change in the case of the slow component τ_2 from 0.7 to 0.5 ns and in the case of τ_1 from 0.1 to 0.2 ns for colored hair. FLIM pattern and lifetime histograms show clearly evidence of eumelanin.

CONCLUSION

The method of multiphoton imaging is able to generate 4D images of autofluorescent hair structures with submicron spatial resolution and picosecond temporal resolution. The recording of the fluorescence lifetime per pixel offers an additional method to analyze both intrinsic and artificial components of the hair without destroying the sample. Biexponential modeling appears sufficient to distinguish between different fluorophores. The fluorescence lifetime maps provide visual information on the intrahair fluorophore distribution. In addition, the analysis of the lifetime distributions based on histograms is another tool to characterize the samples.

It was possible to differentiate between the main fluorescent components of human different hairs eumelanin, pheomelanin, and keratin. Even in samples containing only a minimal amount of melanosomes (white hair) as well as in the case of dyed hairs it was still possible to detect the original hair color.

Multiphoton tomography allows in vivo measurements on intradermal hair components. The long-time high resolution monitoring of the diffusion along hair shafts, the intratissue accumulation and the influence of pharmaceuticals and cosmetical products becomes possible.

REFERENCES

Becker W. 2005. Advanced time-correlated single photon counting techniques. Springer series in chemical physics, Vol. 81. Berlin, Heidelberg, New York: Springer.

Bugiel I, König K, Wabnitz H. 1989. Investigations of cells by fluorescence laser scanning microscopy with subnanosecond resolution. Lasers Life Sci 3:47–53.

Caspers PJ, Lucassen GW, Carter EA, Bruining HA, Puppels GJ. 2001. In vivo confocal Raman microspectroscopy of the skin: Noninvasive determination of molecular concentration profiles. J Invest Dermatol 116:434–442.

Commo S, Gaillard O, Bernard B. 2004. Human hair greying is linked to a specific depletion of hair follicle melanocytes affecting both the bulb and the outer root sheath. Brit J Dermatol 150:435–443.

Corsi M, Cristoforetti G, Hidalgo M, Legnaioli S, Palleschi V, Salvetti A, Tognoni E, Vallebona C. 2003. Application of laser-induced breakdown spectroscopy technique to hair tissue mineral analysis. Appl Optics 42:6133–6137.

Hallégot P, Peteranderl R, Lechene C. 2004. In-situ imaging mass spectrometry analysis of melanin granules in the human hair shaft. J Invest Dermatol 122:381–386.

Hendriks RF, Lucassen GW. 2000. Two photon fluorescence microscopy of in vivo human skin. Proc SPIE 4164:116–121.

König K. 2000. Multiphoton microscopy in life sciences. J Microsc 200:83–104.

König K, Riemann I. 2003. High-resolution multiphoton tomography of human skin with subcellular spatial resolution and picosecond time resolution. J Biomed Opt 8:432–439.

König K, Ehlers A, Stracke F, Riemann I. 2006. In vivo drug screening in human skin using femtosecond laser multiphoton microscopy. Skin Pharmacol Physiol 19:78–88.

Masters BR, So PT, Gratton E. 1997. Multiphoton excitation fluorescence microscopy and spectroscopy of in vivo human skin. Biophys J 72:2405–2412.

Masters BR, So PT, Gratton E. 1998. Multiphoton excitation microscopy of in vivo human skin: Functional and morphological optical biopsy based on three-dimensional imaging, lifetime measurements and fluorescence spectroscopy. Ann NY Acad Sci. 838:58–67.

Richter T, Peuckert C, Sattler M, König K, Riemann I, Hintze U, Wittern KP, Wiesendanger R, Wepf R. 2004. Dead but highly dynamic—The stratum corneum is divided into three hydration zones. Skin Pharmacol Physiol 17:246–257.

Ulrich V, Fischer P, Riemann I, König K. 2004. Compact multiphoton/single photon laser scanning microscope for spectral imaging and fluorescence lifetime imaging. Scanning 26:217–225.

Van Neste D. 2003. Hair science and technology. Tournai, Belgium: Skinterface.

Zahn H. 1984. Feinbau und chemie des haares. Parfümerie und Kosmetik 65:507–594.